physics

MDPI

Article

On the Non-Local Surface Plasmons' Contribution to the Casimir Force between Graphene Sheets

Yan Francescato [1,†], Simon R. Pocock [1,†] and Vincenzo Giannini [2,*]

[1] The Blackett Laboratory, Imperial College London, London SW7 2AZ, UK; yan.francescato@gmail.com (Y.F.); s.pocock15@imperial.ac.uk (S.R.P.)

[2] Instituto de Estructura de la Materia (IEM), Consejo Superior de Investigaciones Científicas (CSIC), Serrano 121, 28006 Madrid, Spain

* Correspondence: v.giannini@csic.es

† These authors contributed equally to this work.

Received: 21 November 2019; Accepted: 10 January 2020; Published: 19 January 2020

Abstract: Herein we demonstrate the dramatic effect of non-locality on the plasmons which contribute to the Casimir forces, with a graphene sandwich as a case study. The simplicity of this system allowed us to trace each contribution independently, as we observed that interband processes, although dominating the forces at short separations, are poorly accounted for in the framework of the Dirac cone approximation alone, and should be supplemented with other descriptions for energies higher than 2.5 eV. Finally, we proved that distances smaller than 200 nm, despite being extremely relevant to state-of-the-art measurements and nanotechnology applications, are inaccessible with closed-form response function calculations at present.

Keywords: graphene plasmonics; casimir forces; nonlocality; vacuum fluctuations

1. Introduction

Casimir forces are rare instances of quantum phenomena in room conditions, typically manifesting as an attractive force between two conducting plates due to vacuum fluctuations [1,2]. These forces are of critical technological importance, as they cause stiction in micro and nano electromechanical systems (MEMS and NEMS) [3]. In addition, they are linked to many surface effects, such as wettability [4] and friction [5], and hold promise as a means to achieve levitation [6].

It has been recognised that surface modes play a crucial role in Casimir forces, which is particularly true for surface polaritons such as plasmons and phonons, where the associated pole in reflectivity dominates the force [7,8]. Because of this property, surface modes are often engineered via nanostructuration as a means to exert some control over and mitigate the strong attraction arising in tiny gaps [9,10]. However, there is another crucial actor in the physics of dispersive forces; namely, the optical non-locality of the materials [11–15]. This effect, also called spatial dispersion because the polarisation field originates from an extended region of space rather than a point, translates into a dependency of a medium response on the wave vector. It can play a major role in the forces, and tends to be underestimated [14,16].

In this letter, we consider two graphene sheets as a case study to explore the importance of non-local surface plasmons in Casimir forces. First we discuss the importance of doping and Drude damping on the forces; then, we study in detail the effects of non-locality. Despite these modes being strongly affected by Landau damping at short separation distances, we observe that interband transitions dominate the force in this regime. Unfortunately, this corresponds to energies where the Dirac cone approximation for the optical response of graphene breaks down, and a different description of the dielectric response should be used for a more accurate analysis.

2. Theoretical Framework and Results

Graphene, the first isolated 2D material, is a honeycomb lattice of carbon atoms exhibiting exceptional physics, ranging from the room-temperature quantum Hall effect to relativistic charge carrying [17]. Its optical properties are particularly enticing thanks to its linear, Dirac cone-like dispersion (see Figure 1a); in fact, that is the driving force in several nanophotonic situations [18–24].

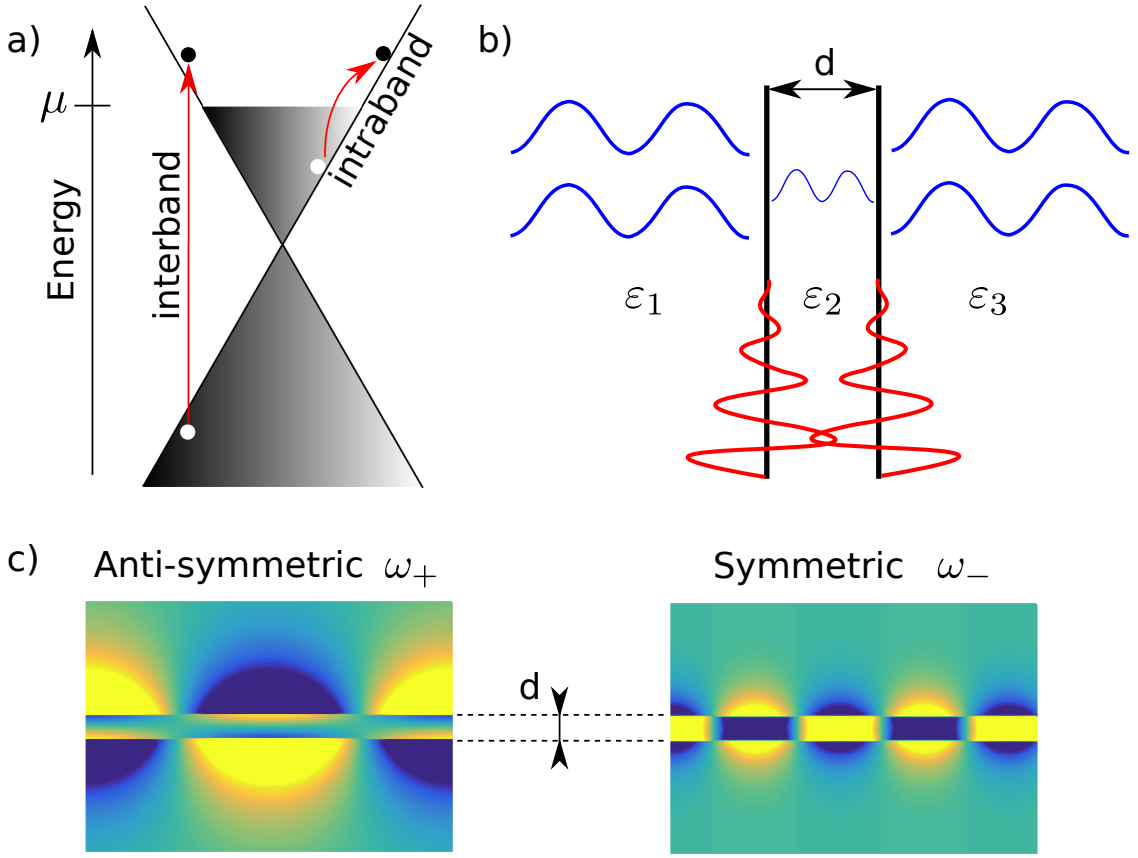

Figure 1. (**a**) Band diagram of doped graphene in the Dirac cone approximation showing interband and intraband transitions at energies $E>$ and $< 2\mu$ respectively. (**b**) Geometry of the graphene sandwich, showing transparency to propagating modes and interaction between highly confined surface plasmons. (**c**) Anti-symmetric (or antibonding) and symmetric (or bonding) plasmon modes between two doped graphene sheets ($\mu = 0.5\,\text{eV}$) separated by $d = 50\,\text{nm}$ at $\hbar\omega = 0.165\,\text{eV}$.

Indeed, this unusual behaviour allows for broadband absorption and is complemented by a large tunability afforded by doping [25]. This tunability enables both interband and intraband transitions, and allows for spectral control over Pauli blocking and Drude response [26].

We are especially interested in graphene because it is mostly transparent to propagating modes, and therefore supports strongly confined surface plasmons. This unique property suggests that the Casimir forces could be solely governed by the plasmonic response. In addition, the 2D nature of graphene allows for a simpler system and implementation, reducing the number of variables considerably, while still manifesting a very rich physics. This makes graphene an ideal platform for the study of Casimir forces.

2.1. Graphene Response

At zero temperature, the non-local susceptibility of a doped graphene sheet with chemical potential $\mu = \sqrt{N\pi}\hbar v_F$ within the random phase approximation can be written as

$$\chi(\omega,k_\parallel)=\frac{2e^2\mu}{\pi\hbar^2v_F^2k_\parallel^2}+ \\ -\frac{e^2}{4\pi\hbar\sqrt{v_F^2k_\parallel^2-\omega^2}}\left[E_+\sqrt{1-E_+^2}+E_-\sqrt{1-E_-^2}+i\,\mathrm{arccosh}\,(E_+)-i\,\mathrm{arccosh}\,(E_-)\right], \tag{1}$$

where $k_\parallel$ is the in-plane wave vector, ω the angular frequency, and $E_\pm=(2\mu\pm\hbar\omega)/\hbar v_Fk_\parallel$ is the rescaled energy change upon absorption (+) and emission (−) of a photon. The prescription $\omega\to\omega+\mathrm{i}0^+$ applies so that the function is analytic in all of the upper complex plane [27]. In Equation (1), the terms in arccosh correspond to the interband transitions taking place at $\hbar\omega>2\mu$, while the terms in $\sqrt{1-E_\pm^2}$ characterise the intraband (Drude) response; see Figure 1a. In order to conserve the number of charge carriers at finite relaxation time $\tau=1/\Gamma$, one must also make use of the Mermin prescription, given by [28]:

$$\chi_\tau(\omega,k_\parallel)=\frac{(1+\mathrm{i}\Gamma/\omega)\chi(\omega+\mathrm{i}\Gamma,k_\parallel)}{1+(\mathrm{i}\Gamma/\omega)\chi(\omega+\mathrm{i}\Gamma,k_\parallel)/\chi(0,k_\parallel)}. \tag{2}$$

When non-locality is ignored, i.e., $k_\parallel\to0$, the susceptibility of graphene can be simply written as

$$\chi(\omega)=-\frac{e^2}{\pi\hbar^2}\frac{\mu}{\omega(\omega+\mathrm{i}\Gamma)}+\frac{e^2}{4\hbar\omega}\left[\mathrm{i}\mathcal{H}(\hbar\omega-2\mu)-\frac{1}{\pi}\log\left|\frac{\hbar\omega-2\mu}{\hbar\omega+2\mu}\right|\right], \tag{3}$$

where $\mathcal{H}$ is the Heaviside function [25]. Again, one can recognise a Drude (intraband) response in the first term, while the second term accounts for interband transitions.

2.2. Lifshitz Formalism

We make use here of the intuitive and elegant theoretical framework developed by Lifshitz [29–31] to calculate the Casimir forces in our planar geometry, which consists of three media separated by two graphene sheets, as shown in Figure 1b. The pressure is obtained by summing all possible electromagnetic modes (evanescent and propagating) via Fresnel reflection coefficients.

Within the Lifshitz formalism for dispersive materials at zero temperature, the Casimir pressure and energy density as a function of the plate separation d can be calculated using real frequencies from

$$P_c(d)=-\frac{\hbar}{2\pi^2}\sum_{\rho=s,p}\int_0^\infty k_\parallel\int_0^\infty\mathrm{Im}\left\{q_2\frac{r_{12}^\rho(\omega)r_{32}^\rho(\omega)}{\mathrm{e}^{2q_2d}-r_{12}^\rho(\omega)r_{32}^\rho(\omega)}\right\}\mathrm{d}\omega\,\mathrm{d}k_\parallel, \tag{4}$$

$$E_c(d)=\frac{\hbar}{4\pi^2}\sum_{\rho=s,p}\int_0^\infty k_\parallel\int_0^\infty\mathrm{Im}\left\{\ln\left[1-\mathrm{e}^{-2q_2d}r_{12}^\rho(\omega)r_{32}^\rho(\omega)\right]\right\}\mathrm{d}\omega\,\mathrm{d}k_\parallel, \tag{5}$$

with ρ, the polarisation; and $q_i(\omega,k_\parallel)=\sqrt{k_\parallel^2-\varepsilon_i(\omega)(\omega/c)^2}$ is the modified normal component of the wave vector in each region. The indices denote the different media, 2 being the gap region and 1 and 3 the left and right-hand half-spaces respectively, as in Figure 1b. The sign convention for the force is that of a negative sign for attraction.

It is often more computationally convenient to calculate the Lifshitz integrals at imaginary frequencies, $\omega=i\xi$, using the form

$$P_c(d)=-\frac{\hbar}{2\pi^2}\sum_{\rho=s,p}\int_0^\infty k_\parallel\int_0^\infty q_2\frac{r_{12}^\rho(i\xi)r_{32}^\rho(i\xi)}{\mathrm{e}^{2q_2d}-r_{12}^\rho(i\xi)r_{32}^\rho(i\xi)}\mathrm{d}\xi\,\mathrm{d}k_\parallel, \tag{6}$$

$$E_c(d)=\frac{\hbar}{4\pi^2}\sum_{\rho=s,p}\int_0^\infty k_\parallel\int_0^\infty\ln\left[1-\mathrm{e}^{-2q_2d}r_{12}^\rho(i\xi)r_{32}^\rho(i\xi)\right]\mathrm{d}\xi\,\mathrm{d}k_\parallel. \tag{7}$$

In this case one needs to make use of modified optical functions for the materials $\varepsilon(i\xi, k_{\parallel})$, $\chi(i\xi, k_{\parallel})$, etc. [32].

Here we consider interfaces covered by graphene, so that the Fresnel coefficients for p (TM) and s (TE) polarization are given by [8,14,16,33]

$$r_{i2}^{s} = - \frac{q_i - q_2 - \mu_0 \omega^2 \chi}{q_i + q_2 - \mu_0 \omega^2 \chi}, \tag{8}$$

$$r_{i2}^{p} = \frac{\varepsilon_2 q_i - \varepsilon_i q_2 + q_i q_2 \chi / \varepsilon_0}{\varepsilon_2 q_i - \varepsilon_i q_2 + q_i q_2 \chi / \varepsilon_0}. \tag{9}$$

2.3. Intrinsic Graphene

In order to understand and correctly trace each contribution to the Casimir forces between graphene sheets, we start by investigating the effects caused by variation in the doping levels of graphene for a broad range of separation distances. Note that as we are interested in gaining physical insights into the phenomena at hand, we restrict ourselves to the case of suspended sheets at zero temperature. Environments different from vacuums result merely in screening, which leads to rescaled forces but no conceptual difference. Similarly, thermal effects bear little consequence for separations below a few tenths of a nanometre [14,16,34], and do not affect the following discussion either. We show in Figure 2 the Casimir pressure normalised to the pressure between two perfect electric conducting (PEC) plates [32] $P_{PEC} = -\hbar c \pi^2 / 240 d^4$.

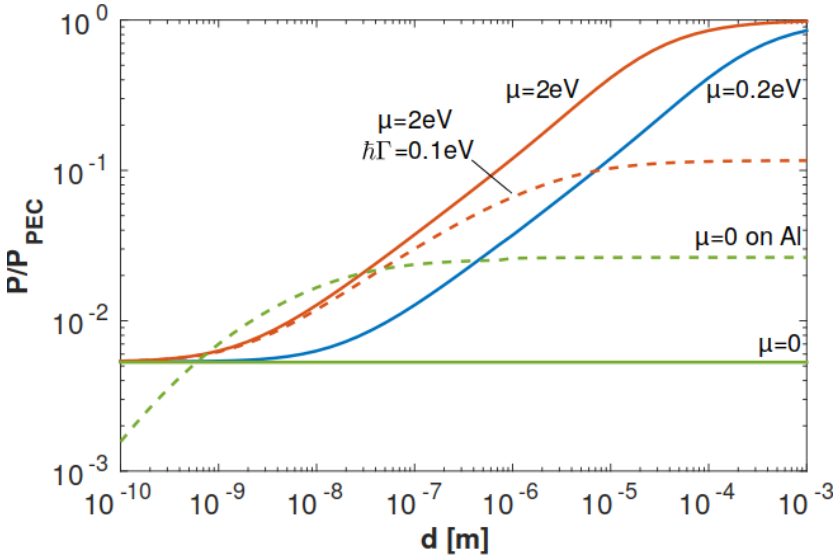

Figure 2. Attractive Casimir pressure between two graphene sheets in a function of distance and normalised to the pressure between two perfect conductors $P_{PEC} = -\hbar c \pi^2 / 240 d^4$. The green line at $P/P_{PEC} \sim 0.00538$ is the force between two intrinsic graphene sheets with universal conductance $\sigma_0 = e^2/4\hbar$. Dashed green is one undoped sheet on top of an aluminium (Drude, $\hbar\omega_p = 12.5\,\text{eV}$, $\hbar\Gamma = 0.063\,\text{eV}$) half-space. Full blue (red) is the force between two doped sheets with $\mu = 0.2\,\text{eV}$ ($\mu = 2\,\text{eV}$) and zero relaxation frequency. Dashed red is the same as red but with Drude damping included ($\hbar\Gamma = 0.1\,\text{eV}$).

First consider intrinsic graphene ($\mu = 0\,\text{eV}$, solid green curve), which is described by the universal conductance [35] $\sigma_0 = e^2/4\hbar = \pi\alpha c\varepsilon_0$. In this case the normalised Casimir pressure is constant [36], with $P/P_{PEC} = 720\alpha/32\pi^3 \sim 0.00538$, where $\alpha = e^2/2hc\varepsilon_0 \sim 1/137$ is the fine structure constant. As we will see later, this behaviour is fully dictated by the assumption that the electronic band structure of graphene is linear; i.e., described by a Dirac cone [35] for all energy transitions. In reality, graphene only takes this particular value in a limited energy range $2\mu < \hbar\omega < 2.5\,\text{eV}$, at which point the Dirac cone approximation breaks down [37].

For comparison, we also show the pressure between such an undoped graphene sheet and an aluminium half-space (dashed green curve), described by a Drude model with $\hbar\omega_p = 12.5\,\text{eV}$ and $\hbar\Gamma = 0.063\,\text{eV}$ [7]. Short distances correspond to high frequencies in the calculation of the force (see Equation (4)), such that the Drude response becomes transparent in the short distance regime, leading to a drastic reduction of the force per unit area. On the other hand, for large separations (relating to low energies), the aluminium becomes a very good metal, approaching the theoretical limit between graphene and PEC [33], with $P/P_{PEC} \sim 0.025$. This simple example shows the importance of the high frequency response of the materials within the Lifshitz formalism at short separations. We return to this central aspect in the last section of the article.

3. Discussion

3.1. Effects of Doping and Loss

When graphene is doped, it becomes more metallic, and one can observe at a larger pressure in Figure 2 for increased doping (solid blue and red lines). However as the distance is reduced, favouring higher energies in the Lifshitz integral, the pressure converges to the case of intrinsic graphene. This is because at sufficiently high energies, the response of graphene is dominated by interband terms, which do not depend on doping, whereas intraband processes are forbidden for $\hbar\omega > 2\mu$ [26]. Therefore, for undoped graphene, only interband transitions contribute. This leads to the universal conductance described above, towards which doped graphene converges at high energies.

We also plot the pressure for a finite scattering rate ($\hbar\Gamma = \hbar/\tau = 0.1\,\text{eV}$, dashed red line), which results in a drastic reduction of the force at large distances but has little effect at short separations. Such Drude damping corresponds to Ohmic losses accompanying the conduction current, which dominates the response of a conductor at low frequencies. As the frequency increases, free carriers start to lag behind the field, and the material response is instead dominated by the polarization field, in which Joule heating plays a negligible role.

3.2. Non-Local Plasmons

To gain a deeper understanding of the effect of plasmons on the pressure, it is helpful to study its spectrum in ωk space, given by the integrand [7] of Equation (4). Several spectra are presented for the case of doped sheets ($\mu = 0.5\,\text{eV}$, $\hbar\Gamma = 0.02\,\text{eV}$, $v_F = 10^6\ \text{ms}^{-1}$) in Figure 3.

In these spectra we can clearly observe the strong poles produced by the surface plasmons, as illustrated in Figure 1c. These confined oscillations of free charges on each sheet couple together to form bonding (or symmetric, ω_-) and anti-bonding (or anti-symmetric, ω_+) hybrids contributing attractively/repulsively to the force respectively [7,8]. Most guided modes give rise to similarly strong contributions [38], and therefore, there is a general interest in trying to use them to control the Casimir force with the help of nanostructuration [9,10].

As the distance is decreased, such as in the step from Figure 3a,b to Figure 3c,d, the increased coupling leads to stronger modes which extend to larger wave vectors. At these shorter distances, non-local effects change the dispersion of the plasmons dramatically, mostly due to Landau damping, which takes place at $\hbar\omega/\mu \geq 2 - k/k_F$ and is clearly visible in Figure 3d. From Figure 3, we can deduce a cross-over in the coupling strength between the plasmons, where the Casimir forces will transition from being governed by Ohmic losses at low frequency and momentum to that of Landau damping when the plasmons are suitably energetic.

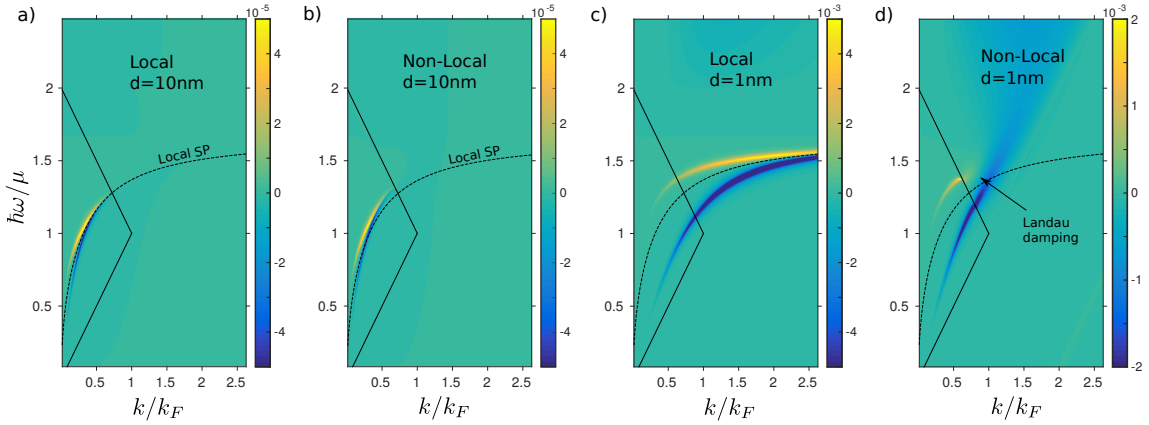

Figure 3. Force per unit area spectrum (in $\mathrm{Ns/m^3}$) of two graphene sheets ($\mu = 0.5\,\mathrm{eV}$, $\hbar\Gamma = 0.02\,\mathrm{eV}$, $v_F = 10^6\,\mathrm{ms}^{-1}$) separated by (**a**,**b**) 10 and (**c**,**d**) 1 nm for the (**a**,**c**) local ($k = 0$) and (**b**,**d**) non-local cases. The axes have been renormalised to $k_F = \mu/\hbar v_F$ and μ respectively. We also plotted as a dashed line, the dispersion relation for uncoupled surface plasmons in the local picture $k_{sp} = -2\varepsilon_0/\chi$.

3.3. Contributions to the Forces

We now turn to the various contributions to the force by separating interband from intraband terms, considering polarisation, and comparing the local and non-local calculations in Figure 4.

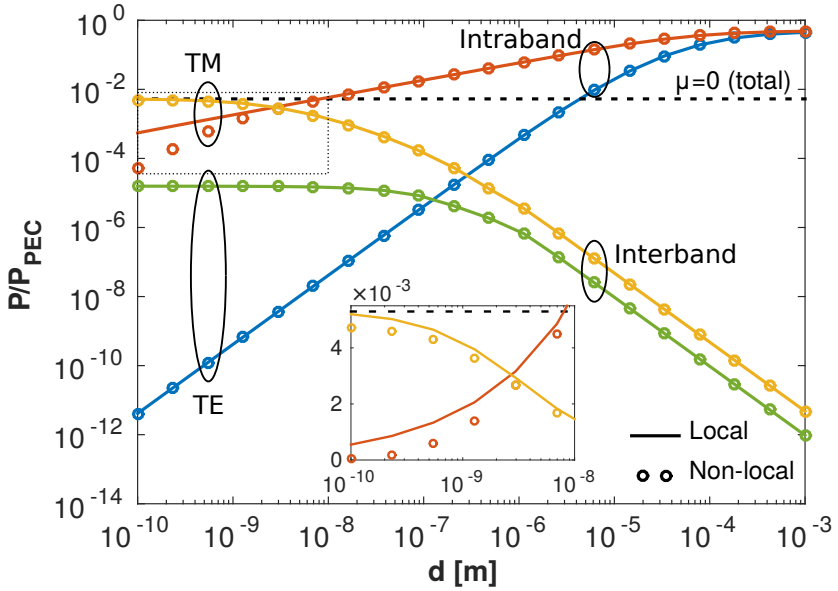

Figure 4. Contributions to the Casimir forces between two graphene sheets ($\mu = 0.5\,\mathrm{eV}$) as a function of the distance and normalised to the pressure between two perfect conductors P_{PEC}. Full lines represent the local case, whereas the circles denote the local situation. The dashed black line is the total force between intrinsic graphene sheets, $P/P_{PEC} \sim 0.00538$. The inset shows the region in the dashed box, where the difference between the local and non-local cases is greatest.

As is well known [14], at large separations both TE and TM modes have a similar strength, originating from waveguided modes within the gap region [39]. In this regime, interband processes are negligible because the relevant energy scale is much smaller than 2μ.

As the distance is decreased, all guided modes (both TE and TM) are cut-off and only surface plasmons, which are TM excitations, are left to contribute to the force. However, the strength of interband transitions also rises strongly at small separations, overcoming that of the intraband response at 2 nm for

the doping considered here ($\mu = 0.5\,\text{eV}$). As discussed earlier, at very short distances the force is mainly due to the interband transitions, and hence the convergence to the case of undoped sheets.

When including the effect of non-locality, displayed as open circles in Figure 4, we observe that mostly TM intraband processes, typically plasmons, are affected. This confirms the intuition derived from Figure 3. These excitations suffer from strong Landau damping at short distances because they correspond to a regime of high phase velocity (momentum), thereby reducing the force compared to the local picture. We can appreciate in the inset of Figure 4 that the non-locality makes a difference in the force spectrum, but it does not in the force.

3.4. Dirac Cone Approximation

Although the previous discussion provides good insight, it ignores a crucial issue related to the Lifshitz formalism in the calculation of the Casimir force. The problem arises from the need to integrate, to infinite frequency, an expression dependent on the susceptibility of graphene.

While the integral converges quickly along imaginary frequencies and can thus be truncated, shorter separations make higher and higher energies relevant. Therefore, the description of graphene must remain valid at these higher energy scales. Unfortunately, the closed-form susceptibility equation we use is only accurate below 2.5 eV, beyond which the Dirac-cone approximation breaks down due to the van Hove singularity and many-body effects, such as excitonic excitations [37,40]. In such a situation we should resort experimental data or more accurate descriptions of the susceptibility. In fact, if the response of graphene was known exactly at all relevant frequencies, the calculation of the force within the general Lifshitz framework should be accurate down to a few angstroms, at which point the evanescent decays of the π orbitals on each graphene sheet start to interact.

In order to illustrate this issue and test the validity of the Lifshitz approach in the case of graphene, we calculated the deviation arising from truncating the integral (Equation (7)). This truncation does not have a physical meaning; its purpose is just to have an idea of the importance of the high energy region on the Casimir effect. The results are shown in Figure 5, where we plotted $\delta E = (E_{truncated} - E_\infty)/E_\infty$ with E_∞ given by Equation (7), and $E_{truncated}$ is the same integral but truncated to $\hbar\omega_{max} = 2\,\text{eV}$ (red lines) or 10 eV (blue lines).

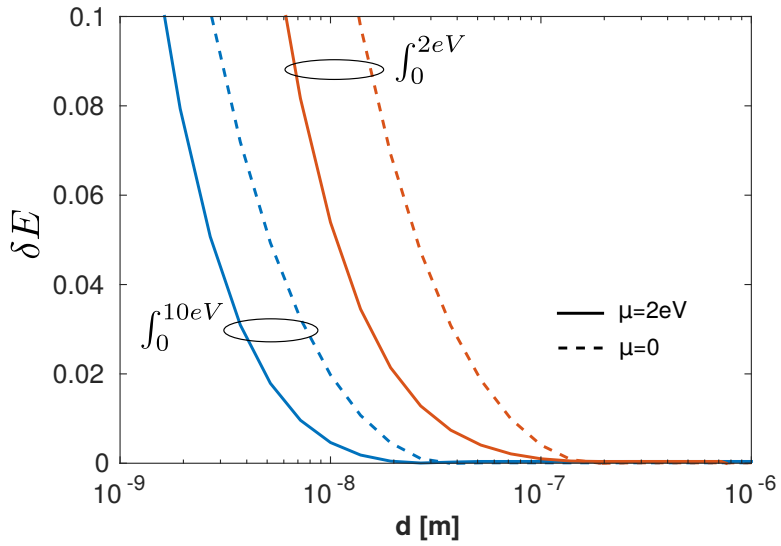

Figure 5. Relative deviation from the Casimir energy when truncating the integral Equation (7) at $\hbar\omega_{max} = 2\,\text{eV}$ (red) or 10 eV (blue) compared to infinity. Dashed lines are for intrinsic graphene sheets and full for $\mu = 2\,\text{eV}$.

It is clear from the dashed lines in Figure 5 that the RPA response used here (Equation (1)) breaks down below 200 nm because it fails to take into account the Van Hove singularity, as discussed earlier. Unfortunately, even a response that would be accurate up to 10 eV, which corresponds to the deep UV,

may not be capable of predictions for distances shorter than a few tens of nanometres. Nevertheless, it would be advisable for calculations made within this energy range to make use of experimental data for the response of graphene as they are certainly more appropriate than the available RPA.

When doping is considered (full lines), intraband excitations are allowed and the weight of the interband term in the integral is decreased, reducing the deviation severalfold for $\mu = 2\,\mathrm{eV}$. This still does not solve the problem of deviation at quite large separations.

4. Conclusions

In this letter, we have revisited Casimir forces between graphene sheets, placing a particular emphasis on their physical origins. To that end we isolated each contribution, explaining in detail the energy range and corresponding separation distances in which they are influential. Furthermore, we made use of the force spectrum representation [7] to highlight the importance of surface plasmons and their dependency on non-locality. We observed that non-local effects do indeed strongly affect these modes at short distances, due to Landau damping. At large separations (low frequency), where a conduction current is prominent in the graphene response, they are instead very sensitive to Ohmic losses.

However, for small gaps, interband transitions dominate because the form of the graphene response considers that they exist, unmodified, to infinity. This arises from the linear dispersion predicted by the Dirac cone approximation, which contradicts experiments [37] for $\hbar\omega > 2.5\,\mathrm{eV}$. By truncating the integral at this value, we showed that this description is unsuited to calculate the Casimir forces between graphene sheets below 200 nm separation distance. This means that there is currently a vast and technologically critical parameter space which is inaccessible by closed-form response function calculations, but of course, this can be fixed using experimental data.

Author Contributions: Y.F. and S.R.P. produced the calculations under the supervision of V.G. and started the manuscript writing. V.G. conceived the project. All authors contributed to the discussion of the results. All authors have read and agreed to the published version of the manuscript.

Funding: V.G. acknowledges the Spanish Ministerio de Economia y Competitividad for financial support through the grant NANOTOPO (FIS2017-91413-EXP) and also the Ministerio de Ciencia, Innovació n y Universidades through the grant MELODIA (PGC2018-095777-B-C21).

Acknowledgments: V.G. acknowledges Ana O'Loghlen for the stimulating discussions.

Conflicts of Interest: The authors declare no conflict of interest.

References

1. Milonni, P.; Shih, M. Casimir forces. *Contemp. Phys.* **1992**, *33*, 313–322. [CrossRef]
2. Lamoreaux, S. The Casimir force: Background, experiments, and applications. *Rep. Prog. Phys.* **2005**, *68*, 201–236. [CrossRef]
3. Capasso, F.; Munday, J.N.; Iannuzzi, D.; Chan, H.B. Casimir forces and quantum electrodynamical torques: Physics and nanomechanics. *IEEE J. Sel. Top. Quantum Electron.* **2007**, *13*, 400–414. [CrossRef]
4. Dellieu, L.; Deparis, O.; Muller, J.; Sarrazin, M. Quantum Vacuum Photon Modes and Superhydrophobicity. *Phys. Rev. Lett.* **2015**, *114*, 024501. [CrossRef] [PubMed]
5. Kardar, M.; Golestanian, R. The "friction" of vacuum, and other fluctuation-induced forces. *Rev. Mod. Phys.* **1999**, *71*, 1233–1245. [CrossRef]
6. Levin, M.; McCauley, A.P.; Rodriguez, A.W.; Reid, M.T.H.; Johnson, S.G. Casimir Repulsion between Metallic Objects in Vacuum. *Phys. Rev. Lett.* **2010**, *105*, 090403. [CrossRef] [PubMed]
7. Henkel, C.; Joulain, K.; Mulet, J.P.; Greffet, J.J. Coupled surface polaritons and the Casimir force. *Phys. Rev. A* **2004**, *69*, 023808. [CrossRef]
8. Pirozhenko, I.; Lambrecht, A. Repulsive Casimir forces and the role of surface modes. *Phys. Rev. A* **2009**, *80*, 042510. [CrossRef]
9. Rodriguez, A.W.; Capasso, F.; Johnson, S.G. The Casimir effect in microstructured geometries. *Nat. Photonics* **2011**, *5*, 211–221. [CrossRef]

10. Rodriguez, A.W.; Hui, P.C.; Woolf, D.P.; Johnson, S.G.; Lončar, M.; Capasso, F. Classical and fluctuation-induced electromagnetic interactions in micron-scale systems: Designer bonding, antibonding, and Casimir forces. *Ann. Phys. (Berl.)* **2015**, *527*, 45–80. [CrossRef]
11. Esquivel, R.; Villarreal, C.; Mochán, W.L. Exact surface impedance formulation of the Casimir force: Application to spatially dispersive metals. *Phys. Rev. A* **2003**, *68*, 052103. [CrossRef]
12. Esquivel, R.; Svetovoy, V.B. Correction to the Casimir force due to the anomalous skin effect. *Phys. Rev. A* **2004**, *69*, 062102. [CrossRef]
13. Sernelius, B.E. Effects of spatial dispersion on electromagnetic surface modes and on modes associated with a gap between two half spaces. *Phys. Rev. B* **2005**, *71*, 235114. [CrossRef]
14. Sernelius, B.E. Retarded interactions in graphene systems. *Phys. Rev. B* **2012**, *85*, 195427. [CrossRef]
15. Luo, Y.; Zhao, R.; Pendry, J.B. van der Waals interactions at the nanoscale: The effects of nonlocality. *Proc. Natl. Acad. Sci. USA* **2014**, *111*, 18422–18427. [CrossRef]
16. Drosdoff, D.; Phan, A.; Woods, L.; Bondarev, I.; Dobson, J. Effects of spatial dispersion on the Casimir force between graphene sheets. *Eur. Phys. J. B* **2012**, *85*, 365. [CrossRef]
17. Geim, A.K.; Novoselov, K.S. The rise of graphene. *Nat. Mater.* **2007**, *6*, 183–191. [CrossRef]
18. Alonso-González, P.; Nikitin, A.Y.; Golmar, F.; Centeno, A.; Pesquera, A.; Vélez, S.; Chen, J.; Navickaite, G.; Koppens, F.; Zurutuza, A.; et al. Controlling graphene plasmons with resonant metal antennas and spatial conductivity patterns. *Science* **2014**, *344*, 1369–1373. [CrossRef]
19. Francescato, Y.; Giannini, V.; Yang, J.; Huang, M.; Maier, S.A. Graphene Sandwiches as a Platform for Broadband Molecular Spectroscopy. *ACS Photonics* **2014**, *1*, 437–443. [CrossRef]
20. Gilbertson, A.M.A.; Francescato, Y.; Roschuk, T.; Shautsova, V.; Chen, Y.; Sidiropoulos, T.T.P.H.; Hong, M.; Giannini, V.; Maier, S.A.S.; Cohen, L.L.F.; et al. Plasmon-induced optical anisotropy in hybrid graphene-metal nanoparticle systems. *Nano Lett.* **2015**, *15*, 3458–3464. [CrossRef]
21. Li, K.; Fitzgerald, J.M.; Xiao, X.; Caldwell, J.D.J.; Zhang, C.; Maier, S.A.S.; Li, X.; Giannini, V. Graphene Plasmon Cavities Made with Silicon Carbide. *ACS Omega* **2017**, *2*, 3640–3646. [CrossRef]
22. Lundeberg, M.B.; Gao, Y.; Asgari, R.; Tan, C.; Van Duppen, B.; Autore, M.; Alonso-González, P.; Woessner, A.; Watanabe, K.; Taniguchi, T.; et al. Tuning quantum nonlocal effects in graphene plasmonics. *Science* **2017**, *357*, 187–191. [CrossRef] [PubMed]
23. Xiao, X.; Li, X.; Caldwell, J.D.J.; Maier, S.A.S.; Giannini, V. Theoretical analysis of graphene plasmon cavities. *Appl. Mater. Today* **2018**, *12*, 283–293. [CrossRef]
24. Galiffi, E.; Pendry, J.; Arroyo-Huidobro, P. Singular graphene metasurfaces. *EPJ Appl. Metamater.* **2019**, *10*. [CrossRef]
25. Koppens, F.H.L.; Chang, D.E.; García de Abajo, F.J. Graphene Plasmonics: A Platform for Strong Light-Matter Interactions. *Nano Lett.* **2011**, *11*, 3370–3377. [CrossRef] [PubMed]
26. Wang, F.; Zhang, Y.; Tian, C.; Girit, C.; Zettl, A.; Crommie, M.; Shen, Y.R. Gate-variable optical transitions in graphene. *Science* **2008**, *320*, 206–209. [CrossRef]
27. Pyatkovskiy, P.K. Dynamical polarization, screening, and plasmons in gapped graphene. *J. Phys. Condens. Matter* **2009**, *21*, 025506. [CrossRef]
28. Mermin, N.D. Lindhard Dielectric Function in the Relaxation-Time Approximation. *Phys. Rev. B* **1970**, *1*, 2362–2363. [CrossRef]
29. Lifshitz, E.M. The theory of molecular attractive forces between solids. *Sov. Phys. JETP* **1956**, *2*, 73–83. Available online: http://www.jetp.ac.ru/cgi-bin/e/index/e/2/1/p73?a=list; Reprinted in *Perspectives in Theoretical Physics: The Collected Papers of E.M. Lifshitz*; Pitaevskii, L.P., Ed.; Pergamon Press Plc: Oxford, UK, 1992; pp. 329–350. [CrossRef]
30. Dzyaloshinskii, I.E.; Lifshitz, E.M.; Pitaevskii, L.P. Van der Waals forces in liquid films. *Sov. Phys. JETP* **1960**, *10*, 161–170. Available online: http://www.jetp.ac.ru/cgi-bin/e/index/e/10/1/p161?a=list; Reprinted in *Perspectives in Theoretical Physics: The Collected Papers of E.M. Lifshitz*; Pitaevskii, L.P., Ed.; Pergamon Press Plc: Oxford, UK, 1992; pp. 425–442. [CrossRef]
31. Dzyaloshinskii, I.E.; Lifshitz, E.M.; Pitaevskii, L.P. General Theory of Van der Waals' Forces. *Sov. Phys. Uspekhi* **1961**, *4*, 153–176. [CrossRef]
32. Klimchitskaya, G.L.; Mohideen, U.; Mostepanenko, V.M. The Casimir force between real materials: Experiment and theory. *Rev. Mod. Phys.* **2009**, *81*, 1827–1885. [CrossRef]
33. Drosdoff, D.; Woods, L.M. Casimir forces and graphene sheets. *Phys. Rev. B* **2010**, *82*, 155459. [CrossRef]

34. Klimchitskaya, G.L.; Mostepanenko, V.M.; Sernelius, B.E. Two approaches for describing the Casimir interaction in graphene: Density-density correlation function versus polarization tensor. *Phys. Rev. B* **2014**, *89*, 125407. [CrossRef]
35. Castro Neto, A.H.; Guinea, F.; Peres, N.M.R.; Novoselov, K.S.; Geim, A.K. The electronic properties of graphene. *Rev. Mod. Phys.* **2009**, *81*, 109–162. [CrossRef]
36. Sernelius, B.E. Casimir interactions in graphene systems. *Europhys. Lett.* **2011**, *95*, 57003. [CrossRef]
37. Mak, K.F.; Shan, J.; Heinz, T.F. Seeing Many-Body Effects in Single- and Few-Layer Graphene: Observation of Two-Dimensional Saddle-Point Excitons. *Phys. Rev. Lett.* **2011**, *106*, 046401. [CrossRef]
38. Intravaia, F.; Lambrecht, A. Surface Plasmon Modes and the Casimir Energy. *Phys. Rev. Lett.* **2005**, *94*, 110404. [CrossRef]
39. Giannini, V.; Zhang, Y.; Forcales, M.; Rivas, J.G. Long-range surface polaritons in ultra-thin films of silicon. *Opt. Express* **2008**, *16*, 19674–19685. [CrossRef]
40. Stauber, T.; Schliemann, J.; Peres, N.M.R. Dynamical polarizability of graphene beyond the Dirac cone approximation. *Phys. Rev. B* **2010**, *81*, 085409. [CrossRef]